Video Integration in a GNSS/INS Hybridization Architecture for Approach and Landing

Jérémy Vezinet, Anne-Christine Escher, Alain Guillet, Christophe Macabiau

HAL Id: hal-00989889

https://enac.hal.science/hal-00989889

Video integration in a GNSS/INS hybridization architecture for approach and landing

Jérémy Vezinet, Anne-Christine Escher,
Christophe Macabiau
ENAC, Telecom Lab
Toulouse, FRANCE

Alain Guillet
AIRBUS
Toulouse, FRANCE

Abstract—**Most of the current operations are supported by the Global Navigation Satellite System (GNSS) potentially augmented with Ground Based Augmentation System (GBAS), Satellite Based Augmentation Systems (SBAS) and Aircraft Based Augmentation System (ABAS). ABAS system integrates on-board information that can for example be provided by Inertial Navigation System (INS) so as to enhance the performance of the navigation system.**

GNSS/INS hybridization is already performed on current commercial aircraft. This solution allows reaching better performance in terms of accuracy, integrity, availability and continuity than the two separated solutions. Hybridization principle is based on the use of GNSS to estimate the inertial drift. It allows navigating in oceanic en-route operations down to non-precision approaches for long range aircraft.

The most stringent requirements for precision approaches or automatic landings cannot be reached with the current GNSS/INS hybridization schemes. In the framework of my PhD stud, the idea is to extend the hybridization filter by including other data available onboard. The global objective of the work is to propose a system that will be able to fuse the multiple sources of information or measurement in a global architecture. The current paper focus on a solution that integrates a video system within an EKF GNSS/INS architecture during approach and landing of an aircraft.

Keywords—Hybridization, Video based navigation, EKF

I. INTRODUCTION

INS/GNSS hybridization is currently used on commercial aircraft in order to compensate drawbacks of the two systems independently. The hybridized solution constitutes a strong, robust, accurate solution for the estimation of most of the navigation parameters. Some solutions also include a integrity monitoring algorithm that can detect GNSS or INS failures. However some operations require new constraints and requirement that can't be achieved with the current navigation solution. In that way, one of the ideas was to use other sources of data and to propose other hybridization architectures.

The study of the possible sensors/systems and associated information/measurements available on board a commercial aircraft has been investigated in previous works, and a set of sensors and data to consider has been identified: a GNSS (potentially augmented with GBAS), an INS (different classes of inertial sensors will be considered) and a video system.

The aim of my work is to arrive to the definition of a global hybridization filter architecture based on the integration of multiple information/measurement sources or sensors (INS, GNSS receiver and a video system), depending on the operational environment: the aircraft operation considered, the sensors available during the considered operation, the performance requirement for supporting the considered operation. In a first part, the current paper, as a first step, will describe an algorithm for integrating optical angular measurements in a classical GNSS/INS Kalman Filter Hybridization solution. The optical angular measurements are supposed to be provided by a camera mounted on-board the aircraft, capable to detect and track features of known location on the runway.

Then, the paper will describe the model for the generation of the optical angular measurements, as well as the mechanization process of the integrated solution that relates the visual measurement and the state of the filter.

Finally, some simulations results of the proposed algorithm will be presented. The simulation results of the filter when integrating video will permit to validate the proposed integration and to constitute a basis for future simulations. Performance assessment is not done in the current paper. The goal is to describe the GNSS/INS EKF architecture and to present a solution for integrating video during approach and landing.

II. EKF ALGORITHM DESCRIPTION

A. EKF Model

The discrete state EKF is described by the following equations:

$$x_k = f(x_{k-1}) + w_{k-1}$$
$$z_k = h(x_k) + v_k \tag{1}$$

Where f and h are respectively the state transition and observation functions, x_k and z_k are respectively the state vector and observation vector at instant k, w_k and v_k are the process and observation noises which are both assumed to be

zero mean Gaussian noises with covariance Q_k and R_k respectively.

Both equations can be linearized with a development in Taylor series. The system then becomes:

$$\delta x_k = F_k \cdot \delta x_{k-1} + w_{k-1}$$
$$\delta z_k = H_k \cdot \delta x_k + v_k \tag{2}$$

Where $F_k = \left.\frac{\partial f}{\partial x}\right|_{x=x_{INS}}$ and $H_k = \left.\frac{\partial h}{\partial x}\right|_{x=x_{k|k-1}}$

The equations of the EKF are then as follows:

Prediction	$\delta \hat{x}_{k|k-1} = F_k \delta \hat{x}_{k-1|k-1}$	(3)
Covariance prediction	$P_{k|k-1} = F_k P_{k-1|k-1} F_k^T + Q_k$	(4)
Gain	$K_k = P_{k|k-1} H_k^T \left(H_k P_{k|k-1} H_k^T + R_k\right)^{-1}$	(5)
Innovation	$I_k = z_k - h\left(\hat{x}_{k|k-1}\right)$	(6)
Update	$\delta \hat{x}_{k|k} = \delta \hat{x}_{k|k-1} + K_k I_k$	(7)
Covariance update	$P_{k|k} = P_{k|k-1} - K_k H_k P_{k|k-1}$	(8)

B. State Transition Model

The EKF state vector is an error state vector that describes the INS error estimation. The state transition model of the EKF implemented has been derived from classic INS mechanization in a wander azimuth coordinate system. This mechanization is done considering an INS composed of 3 accelerometers, 3 gyrometers and a barometer. The INS mechanization also takes into account a 3rd order baro-inertial loop.

The wander azimuth frame is locally defined with respect to the North-Eath-Down (NED) local navigation frame as follows:
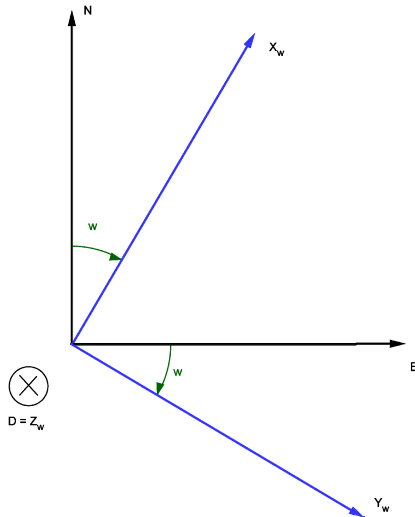

Fig. 1. Definition of the wander azimuth frame

Where the angle w is defined as the wander azimuth angle, its computation is done as described in [5].

Frame definition:

In the entire paper, by convention we will use the following notations for the frame involved:

(X, Y, Z) is the inertial frame (i-frame). It is define as a reference frame in which Newton's laws of motion apply. The origin of the inertial frame is given coincident with the earth's center of mass, the X axis points toward the vernal equinox, the Z axis points along the earth's spin axis and the Y axis is defined to complete the right-handed coordinate system.

(X_e, Y_e, Z_e) is the Earth-centered earth-fixed frame (ECEF-frame or e-frame). Its origin is fixed to the center of the earth. The coordinate axis is fixed to the earth and the Z_e axis is aligned with the Z axis of the inertial frame. Then the ECEF frame rotates relative to the inertial frame at a frequency of $\omega_{e/i} \approx 7.292115 \times 10^{-5}\ rad/s$

(N, E, D) is the Geographic navigation frame (NED-frame or n-frame). The geographic frame is defined locally, relative to the earth's geoid. The Z_n axis points toward the interior of the ellipsoid along the ellipsoid normal. The X_n axis points toward the North and the Y_n axis points east to complete the orthogonal, right-handed frame. The frame origin is the projection of the platform origin onto the earth's geoid. We will use, the ECEF geodetic coordinates system that introduces the latitude, longitude and altitude parameters (λ, ϕ, h).

(X_b, Y_b, Z_b) is the body or mobile frame (b-frame or m-frame). The body frame is rigidly attached to the vehicle of interest, usually at a fixed point such as the center of gravity. The X_b axis is defined in the forward direction. The Z_b axis is defined pointing to the bottom of the vehicle. The Y_b axis is defined pointing to the right of the vehicle in order to complete the right-handed orthogonal frame. All these frames are illustrated in Fig. 2.
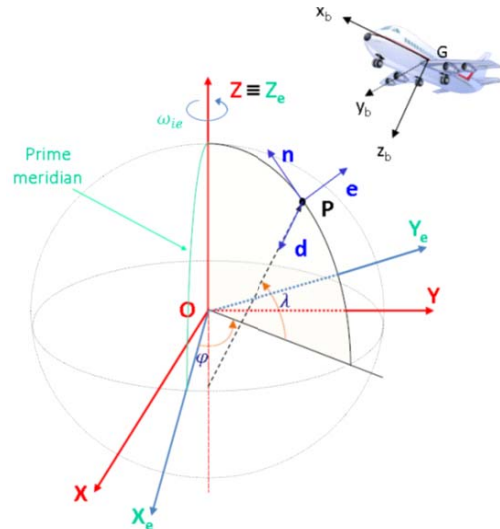

Fig. 2. Coordinate and reference frames [6]

The last frame (X_w, Y_w, Z_w) is the wander azimuth frame (w-frame). Wander azimuth reference frames solve the high latitude problem faced by the geographic frame. The definition is expressed in terms of the angular velocity of the frame with respect to the earth frame. In that way when the instantaneous rotation vector of the w-frame with respect to the e-frame expressed in the n-frame is as follows:

$$\omega_{w/e}^n = \begin{bmatrix} \dot{\phi} \cdot \cos(\lambda) \\ -\dot{\lambda} \\ 0 \end{bmatrix} \quad (9)$$

Velocity error equation:

The INS error mechanization in wander azimuth frame is described by the Earth relative velocity error equation in the wander-azimuth frame [7]:

$$\begin{aligned}
\delta\dot{v}_e^w = \delta f^w + (-\tilde{f}^w \wedge)\rho + \delta g^w \\
+ (\hat{v}_e^w \wedge)(\delta\omega_{w/e}^w + 2\delta\omega_{e/i}^w) \\
- (\hat{\Omega}_{w/e}^w + 2\hat{\Omega}_{e/i}^w)\delta v_e^w
\end{aligned} \quad (10)$$

Where:

- δv_e^w is the Earth-relative velocity error in the wander azimuth system coordinates

- δf^w is the specific force error in the wander azimuth system coordinates (i.e. the accelerometer biases)

- $\tilde{f}^w$ is the measured specific force

- δg^w is the local gravity vector error (in the current study, a Somigliana model is used for the local gravity [7])

- $\hat{v}_e^w$ is the estimated Earth relative velocity expressed in the wander azimuth system coordinates

- $\omega_{a/b}^a$ is the instantaneous rotation vector of the a-frame with respect to the b-frame, expressed in the a-frame coordinate system. $\Omega_{a/b}^a$ is the associated skew symmetric matrix.

Attitude error equation:

The second equation that describes the INS error mechanization is the attitude error equation [7]:

$$\dot{\rho} = -\hat{\Omega}_{w/i}^w \cdot \rho + \hat{R}_{m2w} \cdot \delta\omega_{m/i}^m - \delta\omega_{w/i}^w \quad (11)$$

Where:

- $\dot{\rho} = -\hat{\Omega}_{w/i}^w \cdot \rho + \hat{R}_{m2w} \cdot \delta\omega_{m/i}^m - \delta\omega_{w/i}^w$ is the attitude error vector

- $\delta\omega_{m/i}^m$ is the rotation rate error of the mobile frame with respect to the inertial frame (i.e. the gyrometer biases)

State vector:

The state vector of the implemented filter is as following:

- $d\theta_x, d\theta_y$ are the horizontal angular position error in the wander azimuth frame.

- dh_B is the baro-inertial altitude error.

- da_B is the output of the compensator of the feedback loop of a third order baro-inertial loop.

- dV_x, dV_y are the horizontal velocity error in the wander azimuth frame.

- dV_z is the baro-inertial vertical speed (in along the down vertical axis).

- $d\phi_x, d\phi_y, d\phi_z$ are the alignment angles errors in the wander azimuth frame.

- bg_x, bg_y, bg_z are the gyroscope bias errors in the aircraft frame.

- ba_x, ba_y, ba_z are the accelerometer bias errors in the aircraft frame.

- b_H is the GNSS receiver clock bias error.

- d_H is the GNSS receiver clock drift error.

- $err_{GNSS\,1}, \ldots, err_{GNSS\,N}$ are the GNSS pseudoranges correlated errors (for N satellites).

The linearized state transition matrix F_k is then derived from the INS mechanization as it is done in [8].

The first two states are horizontal angular position error expressed in the wander azimuth frame. These parameters denoted $d\theta_x$ and $d\theta_y$ can be expressed in the NED frame as follows:

$$\begin{aligned}
d\theta_x = d\theta_N \cdot \cos w + d\theta_E \cdot \sin w \\
d\theta_y = -d\theta_N \cdot \sin w + d\theta_E \cdot \cos w
\end{aligned} \quad (12)$$

Then the invert transformation is:

$$\begin{aligned}
d\theta_N = d\theta_x \cdot \cos w - d\theta_y \cdot \sin w \\
d\theta_E = d\theta_x \cdot \sin w + d\theta_y \cdot \cos w
\end{aligned} \quad (13)$$

These horizontal angular position errors (also called "small angles") are related to the errors in latitude and longitude by the following relations:

$$\begin{aligned}
dlat = d\lambda = -d\theta_E \\
dlong = d\phi = \frac{d\theta_N}{\cos\lambda}
\end{aligned} \quad (14)$$

The transition matrix for the biases can be modeled as a first order Markov process with a driven noise and a correlation time that corresponds to the quality of the sensors.

The transition matrix for the GNSS pseudoranges correlated errors can be modeled as a first order Markov with a driven noise and a correlation time that corresponds to the biggest error contribution in the pseudorange measurements.

The transition matrix for the receiver clock is obtained from the two-state clock model as described in [7]:

$$\begin{bmatrix} \dot{b}_H \\ \dot{d}_H \end{bmatrix} = \underbrace{\begin{bmatrix} 0 & 1 \\ 0 & 0 \end{bmatrix}}_{F_{clock}} \cdot \begin{bmatrix} b_H \\ d_H \end{bmatrix} + \begin{bmatrix} n_\phi \\ n_f \end{bmatrix} \qquad (15)$$

C. Observation Model

The observation model is described by the h function and its linearized matrix form F_k. In the global integration architecture presented in the current paper, observations are provided by two systems: a GNSS receiver and a video system. The video system observations and the observation function for video are presented in the next part.

For the GNSS receiver observation, the code pseudorange measurements, we will consider the following measurement model:

$$Pr^i(k) = \rho^i(k) + cb_H(k) + err_{GNSS\,i} + n^i(k) \qquad (16)$$

With:

$$\rho^i(k) =$$
$$\sqrt{\left(X^i(k) - X(k)\right)^2 + \left(Y^i(k) - Y(k)\right)^2 + \left(Z^i(k) - Z(k)\right)^2}$$ is
the geometrical range between the receiver antenna and the ith satellite antenna, c is the speed of light, b_H is the receiver clock bias, $err_{GNSS\,i}$ is the contribution of pseudorange errors correlated in time, and n^i is a white Gaussian noise.

By denoting,

$$h^i_{GNSS}(x_k) = \rho^i(k) + c \cdot b_H(k) + err_{GNSS\,i} \qquad (17)$$

We obtain the following observation model for the ith pseudorange measurement:

$$y^i_k = PR^i(k) = h^i_{GNSS}(x_k) + n^i(k) \qquad (18)$$

Then the linearized observation matrix H^i_{GNSS} only depends on position and receiver clock bias. The three first elements of the matrix are as follows:

$$H^i_{GNSS}(1:3) = \begin{bmatrix} \dfrac{\partial \rho^i}{\partial \theta_x} & \dfrac{\partial \rho^i}{\partial \theta_y} & \dfrac{\partial \rho^i}{\partial h_B} \end{bmatrix} \qquad (19)$$

The other elements are:

$$H^i_{GNSS}(4:N)$$
$$= \begin{bmatrix} 0 & \cdots & 0 & \overset{b_H}{\overset{\frown}{1}} & 0 & 0 & \cdots & 0 & \overset{i^{th}}{\overset{\frown}{1}} & 0 & \cdots & 0 \end{bmatrix} \qquad (20)$$

Where N is the size of the state vector.

The linearized observation matrix for the video observation is detailed in the next part of the paper.

III. VIDEO MEASUREMENT INTEGRATION

A. Video Measurement Model

The video measurements are provided at each instant by a video system composed of a camera and a video processing algorithm.

The camera is supposed to be mounted on the aircraft in order to provide measurements that correspond to features detected in the scenery during approach and landing (runway, airport environment, targets…). A previous study about navigation based on video has been done in [2]. From this study, a model for video measurements has been proposed. This model is composed of a set of two angular coordinates that describes the location of the image of a specific target in the environment. In our study [2], we proposed a scenario where the video system is able to detect and track the corners of the runway during the approach and landing.

The current study is not focused on the detection of the features by an image processing algorithm and made the assumptions that the measurements are directly provided at the output of the video system.

To summarize, the video System is supposed to detect runway corners (with known locations) in the runway environment and to provide for each feature the following data illustrated in Fig. 3:

− A measurement of the angle between the x-axis of the aircraft frame and the Line-of-Sight from the focal point of the camera to the target projected in the vertical plane represented by the x-axis and z-axis of the aircraft frame. The measurement is denoted $\tilde{\alpha}_x$.

− A measurement of the angle between the x-axis of the aircraft frame and the Line-of-Sight from the focal point of the camera to the target projected in the horizontal plane represented by the x-axis and y-axis of the aircraft frame. The measurement is denoted $\tilde{\alpha}_y$.
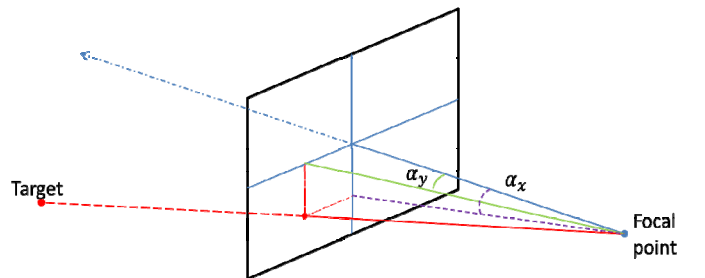

Fig. 3. Optical angular measurements

These angular measurements are converted in metrical measurements that will be used in the observation model as follows for one target:

$$tan(\tilde{\alpha}_x) = tan(\alpha_x) + n_x$$
$$tan(\tilde{\alpha}_y) = tan(\alpha_y) + n_y \qquad (21)$$

Where n_x and n_y are white Gaussian noises that describe the total error on the coordinate of the detected point in the image.

These measurements are related to pixel coordinates of image points as follows:

$$tan(\tilde{\alpha}_x) = \frac{\tilde{X}}{f}$$
$$tan(\tilde{\alpha}_y) = \frac{\tilde{Y}}{f} \qquad (22)$$

Where f is the focal length of the camera.

By denoting,

$$h_{vid}(x(k)) = tan\left(\begin{bmatrix} \alpha_x \\ \alpha_y \end{bmatrix}\right) \qquad (23)$$

$$tan(\alpha_X) = h_1(\lambda, \phi, h_B, \varphi, \theta, \psi)$$
$$tan(\alpha_Y) = h_2(\lambda, \phi, h_B, \varphi, \theta, \psi) \qquad (24)$$

We obtain the following observation model for the video measurements:

$$y_1 = tan(\tilde{\alpha}_x) = h_1(x) + n_x$$
$$y_2 = tan(\tilde{\alpha}_y) = h_2(x) + n_y \qquad (25)$$

B. Video Observation Model

The video observation model is a function that relates the measurement to the state of the system. In order to define the video observation model, we need to find on which states depends the observation function. This observation function will also be used in order to generate the video measurements.

The first and most simple dependency is with the roll angle as it is illustrated in Fig. 4. This figure shows the image observed by a camera during an approach when seeing the runway. The coordinate of the point detected in the image (X, Y) can be related to its coordinate (X', Y') in a horizontal frame (rotated of the roll angle with respect to the image frame).
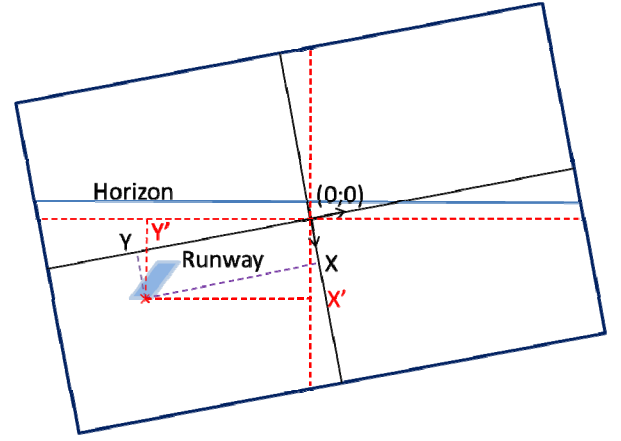

Fig. 4. Impact of roll angle on video measurements

This rotation establishes a relation between the two angular measurements (α_x, α_y) and an intermediate set of coordinates denoted (α'_x, α'_y). The relation is described in (26).

$$tan(\alpha_x) = tan(\alpha'_x)\cos\varphi + tan(\alpha'_y)\sin\varphi$$
$$tan(\alpha_y) = -tan(\alpha'_x)\sin\varphi + tan(\alpha'_y)\cos\varphi \qquad (26)$$

Where φ is the roll angle of the aircraft.

In the following, the dependency of the observation function with pitch, heading and position of the aircraft will be detailed.

The entire description can be illustrated with the Fig. 5. These figures detail the relations between the measurements angles and the aircraft state.

First considering the measurement in the vertical plane, taking into consideration the curvature of the Earth we have the following scheme:
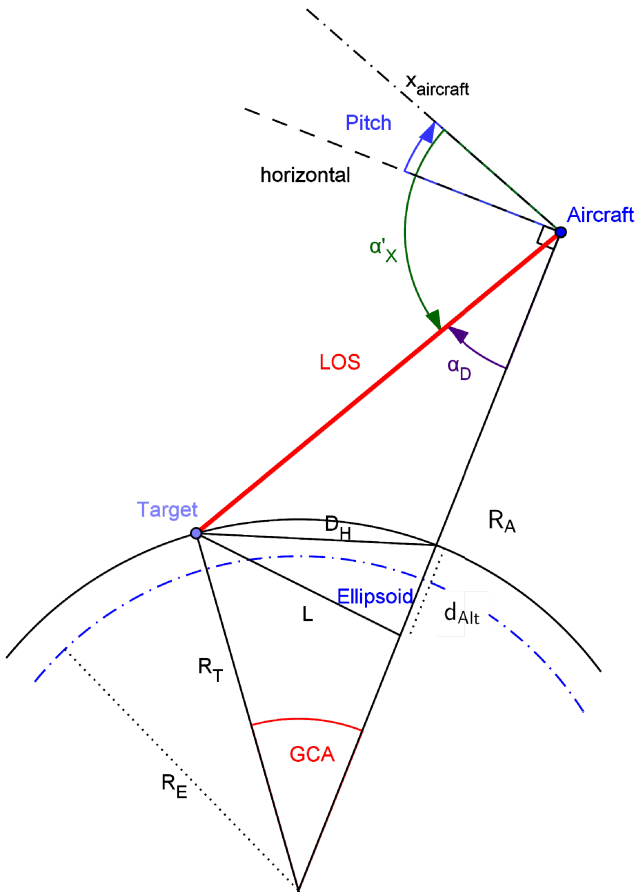
Fig. 5. Observation model for the vertical optical angular measurement

From that figure, we have the following relation:

$$\alpha'_x = \theta + \frac{\pi}{2} - \alpha_D \qquad (27)$$

Where θ is the pitch angle of the aircraft.

Then the relation between the tangents of the angles is as follows:

$$\begin{aligned}\tan(\alpha'_x) &= \tan\left(\theta + \frac{\pi}{2} - \alpha_D\right) \\ &= \frac{1 + \tan\alpha_D \cdot \tan\theta}{\tan\alpha_D - \tan\theta}\end{aligned} \qquad (28)$$

Thus the following relations can be geometrically deduced from the same figure:

$$L = R_T \cdot \sin GCA \qquad (29)$$

$$\begin{aligned}d_{Alt} &= 2 \cdot R_T \cdot \sin^2\left(\frac{GCA}{2}\right) \\ &= R_T \cdot (1 - \cos(GCA))\end{aligned} \qquad (30)$$

$$\begin{aligned}\tan\alpha_D &= \frac{L}{d_{Alt} + \Delta Alt} \\ &= \frac{R_T \cdot \sin(GCA)}{R_T \cdot (1 - \cos(GCA)) + \Delta Alt} \\ &= \frac{R_T \cdot \sin(GCA)}{R_E + h_B - R_T \cdot \cos(GCA)}\end{aligned} \qquad (31)$$

The angle denoted GCA (for Great Circle Angle) can be related to the other parameters with the formula of the haversine function. This function defines the haversine of an angle as following:

$$\begin{aligned}h_a(x) &= \sin^2\left(\frac{x}{2}\right) \\ &= \frac{1 - \cos(x)}{2}\end{aligned} \qquad (32)$$

Using the geometrical law of haversines on a sphere we have the following relation:

$$\begin{aligned}h_a(GCA) &= h_a(\Delta\lambda - \Delta\phi) + \sin\Delta\lambda \sin\Delta\phi \cdot h_a\left(\frac{\pi}{2}\right) \\ &= \frac{1 - \cos\Delta\lambda \cos\Delta\phi}{2}\end{aligned} \qquad (33)$$

An expression of the GCA is then:

$$\begin{aligned}GCA &= 2\arcsin\left(\sqrt{\left(\frac{1 - \cos\Delta\lambda \cos\Delta\phi}{2}\right)}\right) \\ &= \arccos(\cos\Delta\lambda \cos\Delta\phi)\end{aligned} \qquad (34)$$

We can finally relate the tangent of the measurements to the attitude and position of the aircraft using a composition of the different functions presented in equations (27) to (34).

In a second way we will consider the horizontal angular measurement. This measurement is illustrated in Fig. 6.
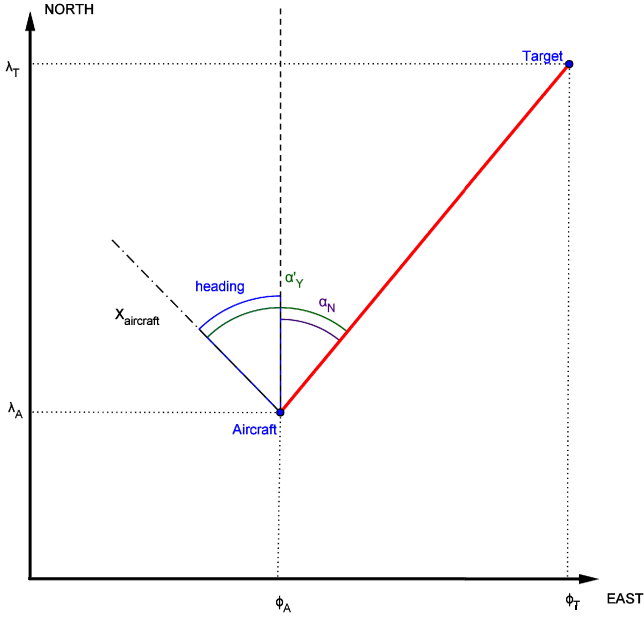
Fig. 6. Observation model for the horizontal optical angular measurement

From that figure, we have the following relation:

$$\alpha_y' = \alpha_N - \psi \tag{35}$$

Then the relation between the tangents of the angles is as follows:

$$\tan(\alpha_y') = \tan(\alpha_N - \psi) \\ = \frac{\tan \alpha_N - \tan \psi}{1 + \tan \alpha_N \cdot \tan \psi} \tag{36}$$

Thus the following relations can be geometrically deduced from the same figure:

$$d_{lat} = 2 \cdot R_T \cdot \sin\left(\frac{\Delta\lambda}{2}\right) \tag{37}$$

$$d_{long} = 2 \cdot R_T \cdot \sin\left(\frac{\Delta\phi}{2}\right) \tag{38}$$

$$\tan \alpha_N = \frac{d_{long}}{d_{lat}} \\ = \frac{\sin\left(\frac{\Delta\phi}{2}\right)}{\sin\left(\frac{\Delta\lambda}{2}\right)} \tag{39}$$

In the same way, we can relate the tangent of the measurements to the attitude and position of the aircraft using a composition of the different functions presented in equations (35) to (39).

C. Linearized Observation Matrix

The linearization of the observation function is done by computation of the Jacobian Matrix of the function. This matrix has two lines for each target and N columns. Each matrix line is as follows:

$$H_{video}^i = \\ \begin{bmatrix} \frac{\partial h^i}{\partial \theta_x} & \frac{\partial h^i}{\partial \theta_y} & \frac{\partial h^i}{\partial h_B} & \frac{\partial h^i}{\partial \phi_x} & \frac{\partial h^i}{\partial \phi_y} & \frac{\partial h^i}{\partial \phi_z} & 0 & \cdots & 0 \end{bmatrix} \tag{40}$$

The computation of the elements of the H matrix is done by using the law of derivation for composition of functions. In fact if we denote:

$$h_1(x, y, z) = x \cdot \cos z + y \cdot \sin z \tag{41}$$

$$h_2(x, y, z) = -x \cdot \sin z + y \cdot \cos z \tag{42}$$

$$f_x(x, y) = \frac{1 + x \cdot y}{x - y} \tag{43}$$

$$f_y(x, y) = \frac{x - y}{1 + x \cdot y} \tag{44}$$

$$g_x(x, y) = \frac{R_T \sin x}{R_E + y - R_T \cos x} \tag{45}$$

$$g_y(x, y) = \frac{\sin\left(\frac{x - \phi_T}{2}\right)}{\sin\left(\frac{y - \lambda_T}{2}\right)} \tag{46}$$

$$k(x, y) = 2 \operatorname{asin}\left(\sqrt{\frac{1 - \cos(x - \lambda_T)\cos(y - \phi_T)}{2}}\right) \\ = \operatorname{acos}(\cos(x - \lambda_T)\cos(y - \phi_T)) \tag{47}$$

These functions can be used in order to describe the entire observation model for the video measurements detailed in the previous part. The computation of the linearized observation matrix needs the computation of a complicate derivation with respect to each state of the state vector. Detailing the derivative of these basic functions can help for the global linearized matrix.

The current part details some elements of the proposed algorithm for the integration of optical angular measurement proposed in [2] in a GNSS/baro-INS architecture. This global integration architecture is done with an EKF. The next part will provide some results obtained with the proposed implementation.

IV. ESTIMATION RESULTS

The current part deals with the presentation of some results of estimation of the proposed EKF. In a first section, only the GNSS/INS architecture is simulated, video is integrated during approach in the second section. In the simulations realized during this study, we used as reference, a set of data recorded

during a real flight. The trajectory performed during this flight is a three hour Toulouse-Toulouse flight. A 3D representation of the trajectory is illustrated in Fig. 7 and the horizontal and altitude profiles are illustrated in Fig. 8.
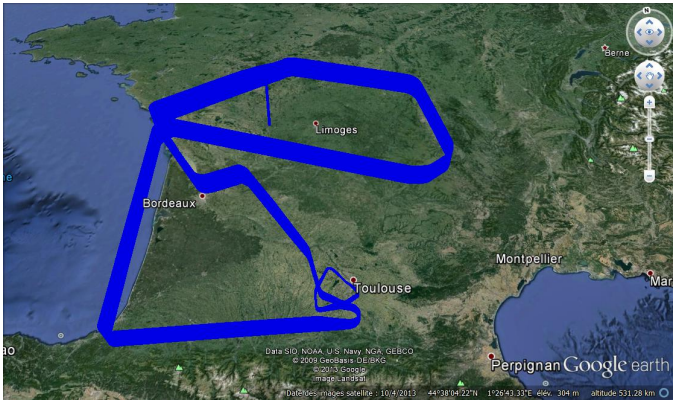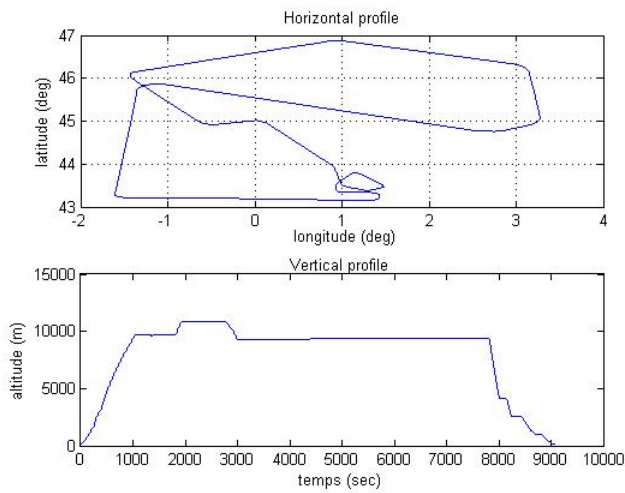

Fig. 7. 3D Trajectory

Fig. 8. Trajectory profiles

As a preliminary step of the global study, inertial measurements were provided by the dataset (more precisely, load factor data were used to generate accelerometer measurements), but we simulated the functioning of a baro-inertial platform (a third order baro-inertial loop). In that way we simulated the baro-inertial estimations of the position, velocity and attitude. It is really important to understand that these first results are obtained from simulated values that could not be completely representative of the reality. The next step of the work will be to do the same simulations using real platform data. This preliminary step is useful in order to validate the complete scenario proposed for the study. In addition, the actual settings of the Kalman Filter (i.e. the values in the transition state covariance matrix and measurement noise covariance matrix) are related to the inertial measurements and to the inertial platform simulator. However they still can be improved. For the next step of the study, new settings will have to be determined in order to match with the real dynamic of the trajectory.

From the position, velocity and attitude parameters recorded during the reference flight and considered as true parameters, we simulate the inertial platform estimations. The aim of the filter was then to estimate the errors made by the simulated inertial platform. After estimation of the inertial errors by the filter, we could compensate the inertial parameters with these estimated errors and then have corrected estimations of the parameters simulated with the inertial platform software.

It can be seen in the following section, that the estimations obtained with the simulated platform does not completely correspond to realistic inertial platform outputs.

The GNSS measurements considered for all the evaluation results presented in this paper are iono-free GNSS/GALILEO measurements. For all these simulations we assumed the nominal 24 GPS constellation, a 27 GALILEO constellation, with 5° mask angle for GPS and 10° mask angle GALILEO, without code carrier smoothing, and unsmoothed measurement error models for tropo, noise, satellite clock and ephemeris as in [9]. Multipath error models are such that L1 and L5 multipath error are uncorrelated with standard deviation $\sigma_{mp} = 0.13 + 0.53 \cdot e^{-\frac{elev}{10}}$ m, assuming airborne multipath errors have a long correlation time.

A. Without Video

The first simulations present result without integrating video in the hybridization architecture. It only consisted in simulations of the GNSS/INS EKF architecture.

As the EKF estimates inertial platform errors, the estimation errors at the output of the platform simulator and at the output of the Kalman Filter are compared. Fig. 9 to Fig. 11 illustrates these differences.
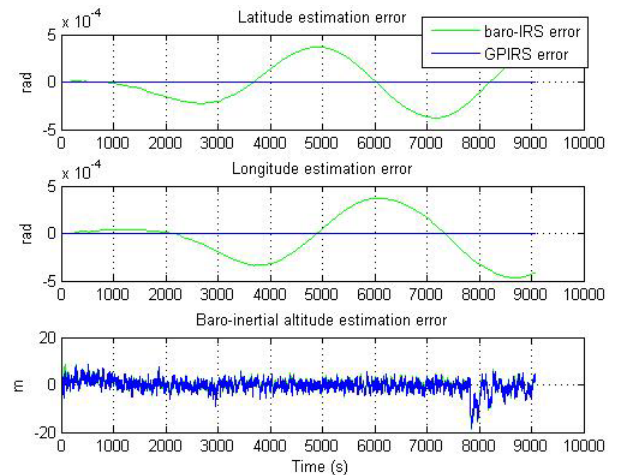

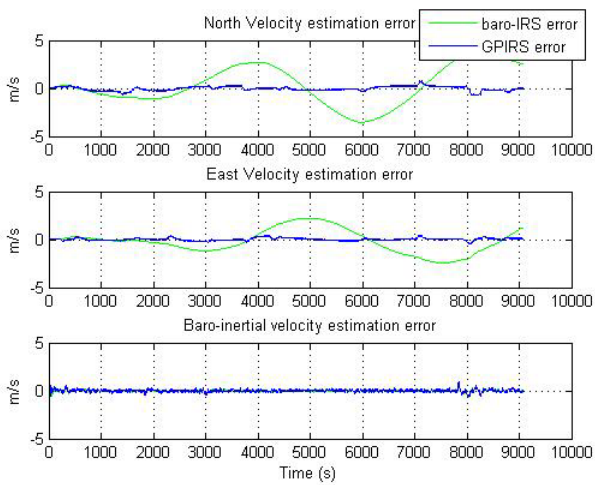Fig. 9. IRS and GPIRS position estimation errors
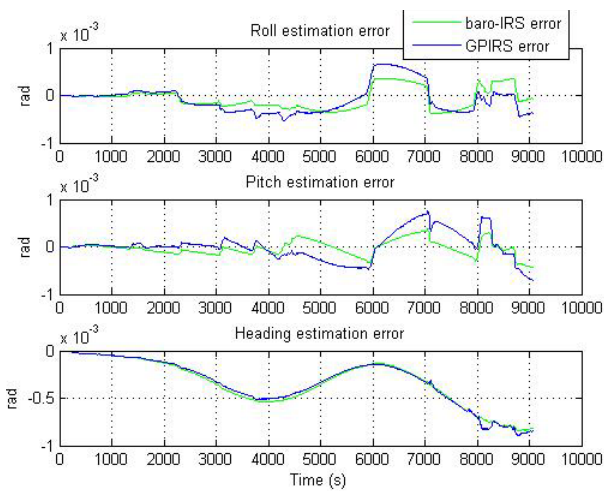
Fig. 10. IRS and GPIRS velocity estimation errors

Fig. 11. IRS and GPIRS attitude estimation errors

From the previous figures, we can see that simulated platform estimations do not illustrate the drifting behavior of a real platform.

In a second step, Fig. 12 to Fig. 14 present the GNSS/INS EKF estimation error of position, velocity and attitude. The estimation errors appear in blue and in red there is the 3-sigma covariance of the estimation error.
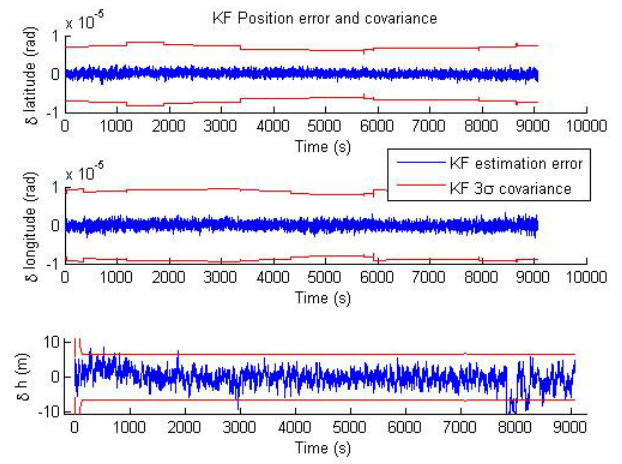

Fig. 12. EKF position estimation error

Horizontal position estimation is improved in comparison with the inertial estimation. The baro-inertial altitude is not improved in that scenario. The horizontal position error estimation is around $10^{-6} rad$. Converting it in meters we obtain a mean value around $6\ m$.
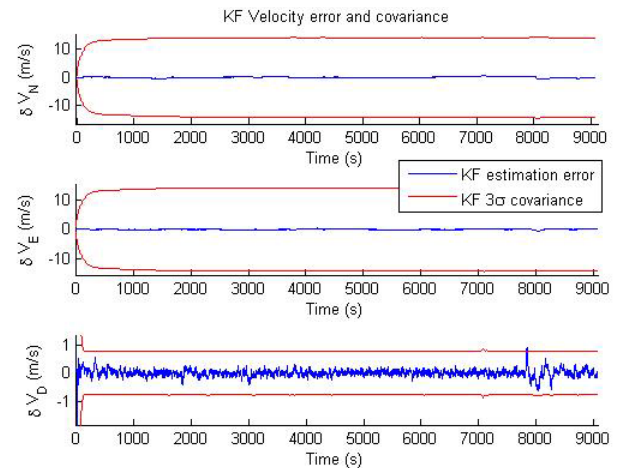

Fig. 13. EKF velocity estimation error

The horizontal velocity error is around $0.2\ m/s$, but the covariance error is much higher. These results can be adjusted by further optimization of the settings of the filter.
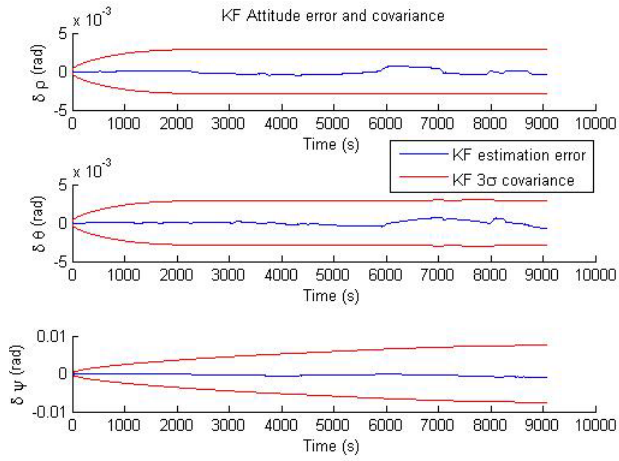
Fig. 14. EKF attitude estimation error

For attitude estimation, the EKF does not bring any improvement. The errors estimated by the EKF do not permit a good correction of the inertial attitude estimation. We could expect this result for attitude estimation because GNSS does not directly provide help for attitude estimation.

The results presented in this section were provided by the GNSS/INS EKF architecture, without video integration. These results show that the filter is able to improve estimation of the navigation parameters. However, the settings still need to be optimized, and the simulated parameters can be replaced by real data. In addition the multipath model for generation of the pseudorange measurements is conservative and not representative of real multipath delays. Next section will provide preliminary results using the video integration process detailed in the previous part of the paper without presenting a performance assessment.

B. With Video

The simulations done in this section only aimed at validating the process proposed for integrating video in a EKF architecture. The video measurements are generated with simulation software developed during this study. It uses the observation matrix described in the previous part. The input parameters of the software are the position and attitude profile of the aircraft on one hand and characteristics of the video system on the other hand. The characteristics are described by three parameters:

– The focal length is set at 5 mm

– The resolution in pixel is set at 2160x4096 (4K)

– The size of the sensor is set at 24x32 mm

Using these parameters and the observation matrix described below, we generate video measurements for two points corresponding at the corners at the beginning of the runway. Their locations are illustrated in Fig. 15. These measurements are available for the final segment of the

approach. Results before integration of video measurements are the same than without video.
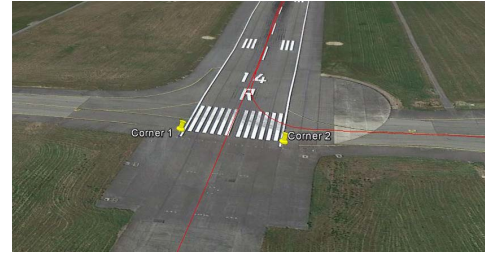

Fig. 15. Corners location

One of the main assumptions used in our study is that the video system is able to detect and lock precise interest points of known locations (corners of the runway). We actually started studies on video processing algorithm in order to try to develop a software able to do such a detection.

Finally, the video measurement simulation generate coordinate in pixels of the detected points in the image. Then these coordinates are turned into the optical angular measurements described in the previous part. Before the conversion a simple error model is added on the pixel coordinates (an error model following a White Gaussian distribution with a standard deviation of 1 pixel). For the following of the study, the error model will be developed.

In addition with the simulation of the video measurements, a "visibility" flag is generated, indicating that the point is actually seen by the camera. In our simulation, this flag is set at 0 when the point is not considered visible and at 1 when it is visible (i.e. when the aircraft is aligned with the runway). In addition we will only consider the approach and landing phases and not the take-off phase.

The results of the estimation of the navigation parameters using video are illustrated in Fig. 16 to Fig. 18.
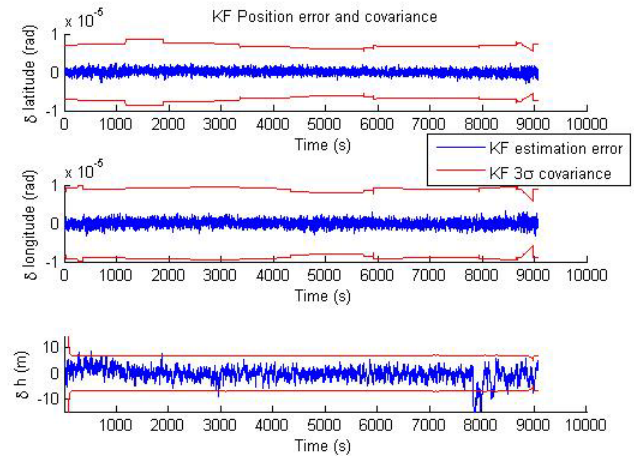

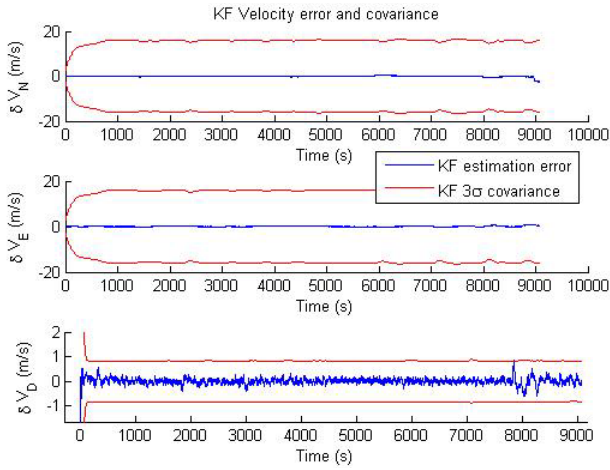Fig. 16. Position estimation with video
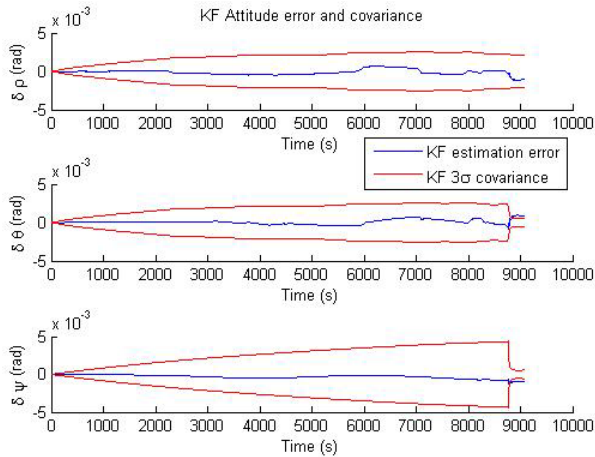
Fig. 17. Velocity estimation with video

Fig. 18. Attitude estimation with video

Analyzing the previous figures presenting the results of the simulations with video, we can first say that there is no significant improvement in terms of accuracy. Attitude seems to be slightly degraded

However, as it is detailed before, the current assumptions of the simulations, which is the use of simulated inertial data, and the use of iono-free GPS/GALILEO measurements does not allow concluding on the improvements provided by the video in term of performance. This part only allows a preliminary validation of the integration of video measurements in the proposed architecture. One of the points that need to be improved is the use of simulated inertial data. In fact, as it is presented in the introduction of the current part, simulated inertial data are used in the current simulations. Also GNSS measurement errors and position errors are very small because we are in the case of iono-free GPS/GALILEO measurements. In that case, the results are not completely representative of the performance of the filter with video measurements. The main objective of the simulations was to validate the video integration architecture, using the video observation model.

In addition, the interest in adding video can be identified by optimizing the settings of the filter.

This is a first step in detailing the improvement provided by video, but the settings of the filter and the parameter of the video will be optimized in the following and the advantage in integrating video when loss a GNSS will be studied. In addition with the optimization of the filter and the video parameters, the use of real data will allows assessing the true performance of integrating video in the current architecture.

As an additional simulation scenario, single frequency GPSL1C or degraded inertial classes can be intended in order to test the integration of video in degraded scenarios.

V. CONCLUSION

Interest in integrating an additional source of data in a navigation algorithm, other than aiding at the estimation of the navigation parameter, is to provide a source of measurement uncorrelated with the GNSS receiver. In fact, the first idea in adding a video system, able to provide visual measurements, was to dispose of another mean for providing information that can be used for navigation purpose. As it was presented in [2], several methods can be used for navigation using video and in that study we wanted to use video as an autonomous means providing absolute geometrical information and in real time (i.e. at each frame of the video). The video process is not supposed to use an external database or reference. This method is supposed to be used during an approach and landing operation, because the runway needs to be visible, then we considered in this study that the visual measurements were available when the aircraft is aligned with the runway.

In the paper we first proposed a hybridization filter using an EKF and integrating video and GNSS code pseudorange measurements. The second part of the paper aimed at detailing the process for integrating the video measurements in the filter. A detailed description of the observation matrix is provided.

Finally some preliminary results, using simulated inertial data and iono-free GPS/GALILEO simulated data, showed that with the actual settings of the filter and characteristics of the video measurements, the video does not provide a significant improvement in terms of accuracy. One of the reasons of the lack of evidence of the improvement brought by video in the current results is that the use of the INS simulated data does not completely produce the real performance in terms of estimation of the navigation parameters. The use of simulated data allows matching the real dynamic of an aircraft and producing the same behavior than a Kalman filter. Also GNSS measurement are iono-free GPS/GALILEO measurements, reflecting a post 2020 situation but with a highly conservative multipath error model that can be refined. In that way, the integration of video in that scenario seems not to provide improvements. However, the interest of this study is that it gives an idea of the process for integrating an additional source of data in a global architecture. This constitutes a good approach for integrating various sensors in a future global hybridization architecture.

These results illustrated the ability of the proposed architecture to integrate other measurements provided by other sources. Further simulations have to be done in that way. This architecture can also be completed with other sensors and the filter model can be modified in order to test some particular

Kalman filters: the Unscented Kalman Filter (UKF) or the Information Kalman Filter (IKF).

For the following of the study, the settings of the filter will be optimized and the parameters of the camera will be refined. The main change in the future simulations will be the use of a set of real data of the same trajectory, in order to assess the real performance of the current architecture.

The existing simulator will also allow us to try some combinations of sensors during approach and landing and during specific scenarios or failure cases. In that way degraded inertial classes an GNSS receivers will be tested. In particular, our study will also test the ability of the video measurements to compensate a GNSS outage and allows performing the current operation.

REFERENCES

[1] GEAS, "Phase I of the GNSS Evolutionary Architecture Study", 2008.

[2] J. Vezinet, A-C. Escher, A. Guillet, C. Macabiau, "State of the Art of Image-Aided Navigation Techniques for Approach and Landing", ION ITM 2013, San Diego, CA.

[3] J. Veth, J. F. Raquet, "Fusion of Low-Cost Imaging and InertialSensors for Navigation", ION GNSS 2006, Fort Worth, TX.

[4] J. Kelly, S. Saripalli, G. Sukhatme, "Combined visual and inertial navigation for an unmanned aerial vehicle", Field and Service Robotics, 2008.

[5] W. A. Poor, "A Geometric Description of Wander Azimuth Frames", Center for Naval Analyses, Alexandria, Virginia, 1989.

[6] A-C. Escher, "Inertial Navigation and GPS/IRS Hybridization", ENAC courses, 2013.

[7] J. A. Farrel, M. Barth, "The global positioning system and inertial navigation", 1999.

[8] J. W. Diesel, "GPS/INS integration for civil aviation", Telesystems Conference, 1991.

[9] L. Montloin, L. Azoulai, A. Martineau, C. Milner, C. Macabiau, "GNSS Multipath Failures Modes Analysis for Airport Surface Operations", ION GNSS 2013